Heat and Mass Transfer (2019) 55:1371–1385
https://doi.org/10.1007/s00231-018-2520-2

ORIGINAL

Modeling of heat transfer through a liquid droplet

Vishakha Baghel[1] · Basant Singh Sikarwar[1] · K. Muralidhar[2]

Received: 11 July 2018 / Accepted: 2 November 2018 / Published online: 14 November 2018
© Springer-Verlag GmbH Germany, part of Springer Nature 2018

Abstract

In dropwise condensation, the released latent heat passes through the static and sliding droplets to the condensing surface at a rate limited by various thermal resistances. In the present work, numerical simulation of heat transfer through a droplet is carried for one under static and sliding condition. 3-D governing equations with appropriate boundary conditions are solved for the surface, promoter layer and droplet included within the computational domain. Simulations are carried out using an in-house CFD solver. The simulation results are validated against the available data and are found in good agreement. The observations of the present work are: (a) heat transfer through the droplet achieves steady state over a timescale of micro-seconds, (b) the heat fluxes of deformed and equivalent spherical-cap droplet are found to be equal, (c) Marangoni convection is significant for Ma ≥ 2204, (d) convection is the dominant mode of heat transfer during drop slide-off (e) constriction resistance is insignificant for a copper surface of thickness ≤ 2 mm, (f) average heat flux increases with increasing contact angle, interfacial heat transfer coefficient, degree of subcooling and Reynolds number; however, it decreases with increasing Prandtl number of the liquid. These results are useful for sensitivity analysis of various thermal resistances in the mathematical modeling of dropwise condensation underneath inclined surfaces.

Nomenclature

a	Base radius of the droplet (m)
$d\sigma/dT$	Surface tension gradient (N/m-K)
$(\partial T/\partial x_i)_s$	Temperature gradient vector at the condensing surface (K/m)
g	Gravitational acceleration (m/s^2)
h_i	Interfacial heat transfer coefficient (W/m^{2}K)
h_{lv}	Latent heat of vaporization (J/kg)
K	Thermal conductivity (W/m-K)
L	Height of the droplet (m)
M	Molecular weight of vapor (kg/mol)
P_v	Vapor pressure (Pa)
q	Average heat flux (W/m^2)
q_l	Local heat flux (W/m^2)
Q	Heat transfer through droplet (W)
r	Radius of the droplet (m)
$\overline{R}$	Universal gas constant (J/mol-K)
R_{cap}	Capillary resistance (K/W)
R_{coat}	Promoter layer resistance (K/W)
R_{cond}	Conduction resistance (K/W)
R_{const}	Constriction resistance (K/W)
R_{conv}	Convection resistance (K/W)
R_{int}	Interfacial resistance (K/W)
R_{ma}	Marangoni resistance (K/W)
R_{th}	Thermal resistance (K/W)
t	Time (sec)
T	Temperature (K)
T_{cap}	Temperature near droplet interface (K)
u	Fluid velocity in x-direction (m/s^2)
v	Fluid velocity in y-direction (m/s^2)
V	Droplet volume (μl)
w	Fluid velocity in z-direction (m/s^2)
x,y,z	Cartesian Co-ordinate

Greek symbols

α	Thermal diffusivity (m^2/s)
β	Interface location (degree)
ΔT	Degree of sub-cooling (K)
ρ	Density of condensate (kg/m^3)
θ	Contact angle (degrees)
δ	Thickness (m)
σ	Surface tension (N/m)
$\hat{\sigma}$	Condensation coefficient
μ	Dynamic viscosity (kg/m-s)
τ	Shear stress (N/m^2).

✉ Basant Singh Sikarwar
bssikarwar@amity.edu

[1] Department of Mechanical Engineering, Amity University, Noida, India

[2] Department of Mechanical Engineering, Indian Institute of Technology Kanpur, Kanpur 208016, India

Non-dimensional parameters

Bi Biot Number, $h_i a/K$
Bo Bond Number, $\Delta\rho g r^2/\sigma$
Ma Marangoni Number, $(-d\sigma/dT\times\Delta T C_p L\rho)/K\mu$
Pr Prandtl Number, $\mu C_p/K$
Re Reynolds Number, $\rho uL/\mu$

Subscripts

c Properties at promoter layer
sat Properties at saturation condition
w Properties at condensing surface

1 Introduction

Condensation is a phase change process in which vapor condenses on the cold condensing substrate either in form of a film and/or a droplet. It has significant applications in industrial processes such as distillation, HVAC, desalination, heat exchangers, power plants, refrigeration systems and water harvesting via dewing [1–4]. Dropwise condensation gained popularity as compared to filmwise condensation when Schmidt et al. [5] reported that the heat transfer coefficient of dropwise condensation is an order higher than filmwise condensation. This attribute of dropwise condensation make it suitable for heat transfer enhancement and energy conservation perspectives [6, 7]. In dropwise condensation, heat is transferred from droplet to condensing surface via three mechanisms [8]. In these mechanisms, the mechanism of droplet formation at specific nucleation sites while the area between the growing drops remains inactive is the most pragmatic mechanism of heat transfer wherein, vapor condense at specific nucleation sites of the substrate in the form of droplets [9]. Later, these droplets grow via direct condensation and coalesce with the neighboring droplets till they become large enough to slide-off/fall-off by body forces [10]. The slide-off/fall-off and coalescence phenomena cleans the condensing surface and allows re-nucleation. Hence, dropwise condensation is cyclic in time [10].

In the drop groth via direct condensation, the vapor condenses on the droplet interface and latent heat is released [11]. The released latent heat passes through the droplet to condensing surface which is limited by various thermal resistances [10], as shown in Fig. 1. These are constriction resistance (R_{const}), drop promoter layer resistance (R_{coat}), conduction resistance (R_{cond}), interfacial resistance (R_{int}) and capillary/curvature resistance (R_{cap}), as shown in Fig. 1 (a). Some researchers [12] showed the presence of Marangoni resistances (R_{ma}) during heat transfer through a static droplet. However, some researchers [13] showed convection heat transfer is dominant mode of heat transfer when droplets slide-off from the condensing surface. Therefore, Marangoni resistances acts parallel to the conduction resistance when droplet is static, as shown in Fig. 1b. Though, Marangoni and convection resistances (R_{conv}) act parallel to the conduction resistance when droplet slide-off, as shown in Fig. 1c. Aforementioned resistances are significant at various stage of droplet evolution in dropwise condensation. The significance of these thermal resistances is summarized as follow:

Constriction resistance occurs because of non-homogeneous and finite thermal conductivity of the condensing surface [10]. However, this resistance is neglected in most of prior studies [14] by assuming uniform temperature distribution on the condensing surface.

Generally, metallic surfaces have high surface energy with respect to water. Consequently, condensation occurs in these surface in form of film [15]. In literature [16, 17] special long chain hydrocarbon on these surfaces are coated to promote condensation in form of droplets. These coatings have very low thermal conductivity and they augment a resistance called drop promoter layer resistance. This resistance is ignored in most of the prior art due to nano-micro scale roughness of the drop promoter layer [18–20].

The condensed liquid droplet itself acts as resistance to heat conduction through the droplet to the condensing surface. This resistance is called as conduction resistance and most of the studies [21] showed that it is the most dominant resistance as compared to other resistances during heat transfer through the droplet in dropwise condensation. Although, it is dominate resistance, prior studies [22–24] derived it expression in various ways in the modeling of heat transfer through the liquid droplet. Le Fevre and Rose [25] derived its expression by assuming a droplet of hemispherical shape. However, Sikarwar et al. [26] derived its expression by assuming spherical cap droplet. Kim et al. [27] derived its analytical expression by considering two neighboring isothermal surfaces close to condensing surface for droplet of contact angle >90°. Later, this expression was adopted by many researchers and scientists [28–32] for developing mathematical model of heat transfer through a single droplet.

Interfacial and capillary resistances act at the droplet interface because of the finite amount of temperature and pressure difference at the droplet interface [10]. At interface, there is transport of molecules crossing the liquid-vapor interface in both direction. For energy exchange between the incoming and departing molecules, a sufficiency condition is required. Net condensation will occur only if a finite temperature difference exists between the liquid-vapor interface and the solid surface. However, capillary resistance occurs because of the pressure difference due to droplet curvature and causes depression in the equilibrium interface temperature below the normal saturation temperature at the liquid-vapor interface [33].

Surface tension gradient leads to thermocapillary Marangoni convection inside the liquid droplet giving rise to Marangoni resistance. The spatial variation in surface tension causes imbalanced shear forces that drive a circulatory flow inside the droplet, from a region of high surface tension (lower temperature) to a region of lower surface tension (high

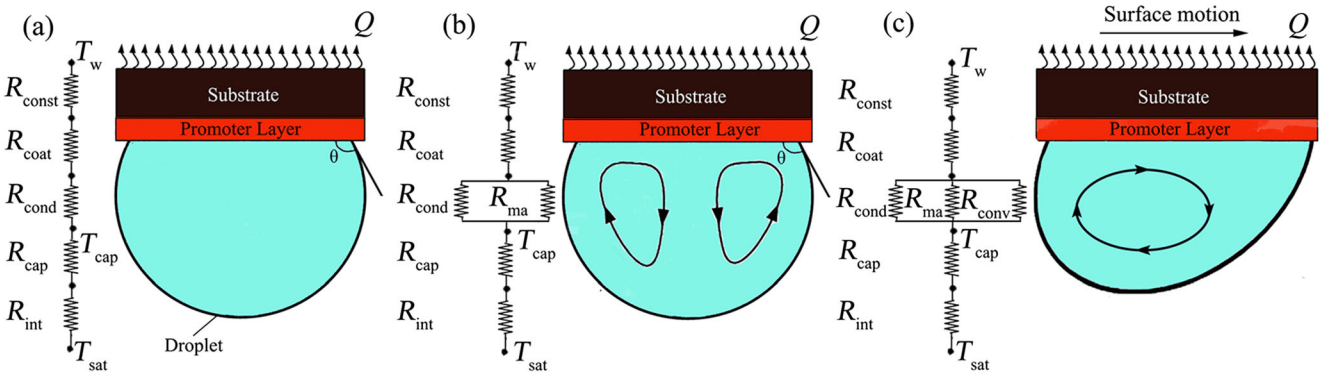

Fig. 1 Schematic diagram of a thermal resistance network for heat transfer through a single liquid droplet; (**a**) without Marangoni convection, (**b**) with Marangoni convection and (**c**) thermal resistances during droplet instability

temperature). The strength of thermocapillary convection is quantitatively estimated from the non-dimensional Marangoni number [34]:

$$Ma = -\frac{d\sigma}{dT} \times \frac{\Delta T C_p L \rho}{K \mu} \tag{1}$$

Here, $d\sigma/dT$ is the surface tension gradient, 'ΔT' is temperature difference between the condensing surface and vapor (degree of sub-cooling), 'L' is the height of droplet, considered as characteristic length, 'ρ', 'K' and 'μ' are density, thermal conductivity and dynamic viscosity of the liquid droplet respectively.

Although each of these resistances are substantial during drop evolution, many prior studies [35, 36] have not considered all resistances in the mathematical expression for heat transfer through single droplet to condensing surface. Chavan et al. [14] performed a 2D axisymmetric numerical simulation for heat transfer through the droplet by considering conduction and interfacial resistances alone. Adhikari et al. [37] considered conduction, interfacial and capillary resistances. Kim et al. [27] and Bahrami et al. [32] considered interfacial, conduction, capillary and promoter layer resistances. Phadnis et al. [12] considered thermocapillary Marangoni convection. Sikarwar et al. [13, 26] considered all the thermal resistances except Marangoni and constriction resistances. To the knowledge of the authors, there is no work available in literature that has considered all thermal resistances during heat transfer through single static and sliding droplet of various shapes and sizes. Negligence of any aforementioned resistances reduces the sensitivity of the mathematical model of heat transfer through the droplet [38].

Against this background, the heat transfer through single droplet in static and sliding state is numerically simulated by considering all the thermal resistances. Unsteady, three dimensional, coupled Navier-Stokes and energy equations are solved with the condensing surface, promoter layer and the liquid droplet within the computational domain. At the condensing surface, Dirichlet and no-slip boundary conditions are specified. Robin-Mixed boundary condition and Marangoni stresses are specified at the droplet interface. A finite

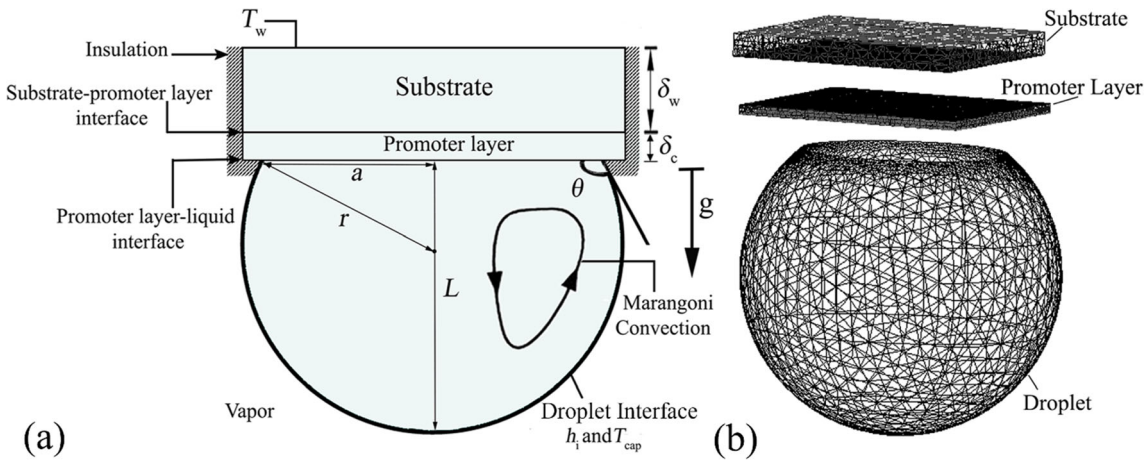

Fig. 2 (**a**) Schematic diagram of droplet underneath a metallic condensing surface with a drop promoter layer. The appropriate boundary conditions are: (i) Dirichlet boundary condition ($T = T_w$) and no-slip at the top of the substrate. (ii) Robin boundary condition (HTC = h_i) with droplet interface temperature ($T = T_{cap}$) and Marangoni stresses at the droplet interface. (**b**) Exploded view of computation domain meshed with tetrahedra in the volume and triangular elements over the surfaces

Table 1 Thermo-physical properties of the condensing surface and drop promoter layer [42, 43]

S. No.	Sub-domain	Material	Density (Kg/m^3)	Specific heat (J/Kg-K)	Thermal conductivity (W/m-K)	Thickness
1	Surface	Al	2702	879.04	180	1-5 mm
		Cu	8933	385	401	1-5 mm
2	Promoter layer	long chain hydrocarbon coating	764.64	3100	0.05–0.2	0.1–100 μm

volume-based in-house CFD solver is used for solving the coupled system of partial differential equations. The liquid droplets considered in the simulation are liquid sodium, water and ethylene glycol. The choice of these fluids as the working fluid is motivated by the range of applications where these fluids are encountered. The simulated results are validated against the data available in literature [14, 27]. Post-validation, time scale to reach steady state during heat transfer through a liquid droplet with and without Marangoni is estimated. Heat fluxes through undeformed and deformed droplets are compared. Further, the effects of various parameters on heat transfer through the single droplet are investigated. The parameters under consideration are droplet volume, thermophysical properties of the liquid droplet, contact angle, interfacial heat transfer coefficient, degree of sub-cooling, substrate thickness and thermal conductivities of the drop promoter layer and the condensing surface. These results are applicable to a droplet ensemble as in a continuous quasi-steady dropwise condensation and for estimating the growth rate of a droplet in a mathematical model of dropwise condensation underneath inclined surfaces.

The text below is arranged in following manner. Section 2 of the paper describes the mathematical formulation and numerical scheme with the details of the implementation of the all resistances, boundary conditions and initial condition over the condensing surface and droplet interface. Results and discussion along with grid independence and code validation are described Section 3. Finally, the conclusions of the study are reported in Section 4.

2 Mathematical formulation and numerical solution

In this numerical formulation, the computational domain has three sub-domains namely condensing surface of thickness δ_w, drop promoter layer of thickness δ_c and a liquid droplet, as shown in Fig. 2a. The shape and size of spherical cap droplet is estimated using Eqs. (2–6) however, the shape and size of deformed droplet is estimated using two-circle approximation [39, 40].

$$V = \frac{\pi r^3}{3}\left[2-3\cos\theta+\cos^3\theta\right] \tag{2}$$

$$L = a\tan\frac{\theta}{2} \tag{3}$$

$$a = r\sin\theta \tag{4}$$

$$A_{sl} = \pi r^2\left[1-\cos^2\theta\right] \tag{5}$$

$$A_{lv} = 2\pi r^2\left[1-\cos\theta\right] \tag{6}$$

Table 2 Thermo-physical properties of liquids studied [10, 38, 44]

Property	Sodium	Water	Water	Ethylene glycol
Prandtl number (Pr)	0.006	4.32	7.56	189.52
Saturation temperature, T_{sat} (K)	500	313	290	295
Wall temperature, T_W (K)	490	303	280	285
Liquid density, ρ_l (Kg/m^3)	898	992.1	999	1116.6
Vapor density, ρ_v (Kg/m^3)	2.20e-05	1.225	1.225	2.5725
Latent heat of vaporization, h_{lv} (kJ/Kg)	4470	2406.9	2461.4	858.3
Surface tension, σ (N/m)	0.175	0.07	0.0737	0.048
Thermal conductivity, K (W/m-K)	81.503	0.631	0.598	0.25
Molecular weight, M (Kg/Kmol)	23	18.02	18.02	62.07
Dynamic viscosity, μ (g/cm-s)	0.00426	0.00653	0.0108	0.202
Condensation coefficient, $\hat{\sigma}$	0.6	0.04	0.04	0.17
Specific heat, C_p (J/Kg-K)	1230	4179	4184	2345.5

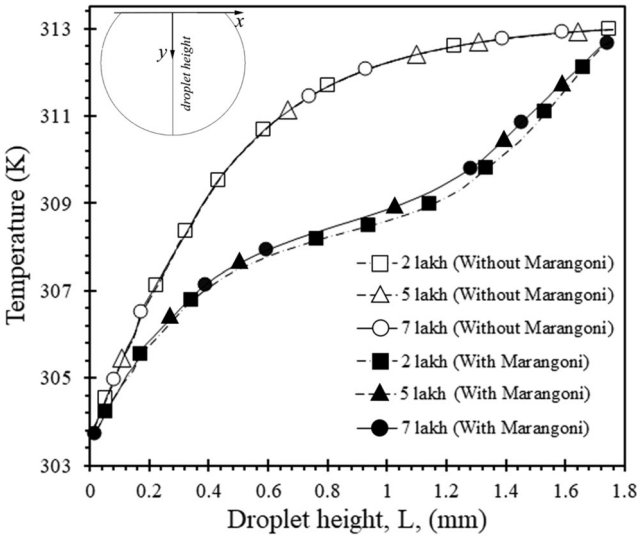

Fig. 3 Temperature profile at midline of droplet (*x*-*y* plane, $z = 0$) with respect to the vertical coordinate for various grid sizes ranging from 2×10^5 to 7×10^5 representing coarse to fine mesh respectively. Grid independence test was performed with and without Marangoni convection inside a single water droplet of contact angle (θ) = 140°, V = 40 μl, T_{sat} = 313 K, ΔT = 10 K, $\hat{\sigma}$ = 0.04, $d\sigma/dT = -0.13$ mN/m-K, δ_w = 2 mm, δ_c = 10 μm, K_c = 0.2 W/m-K and K_w = 401 W/m-K

Here, '*r*' is the radius, '*L*' is the droplet height, '*a*' is the base radius and 'θ' is the contact angle of liquid droplet.

Figure 2b shows the meshing of computational domain in which all the sub-domains are subdivided into small number of tetrahedral elements as control volume in unstructured manner. These control volumes are smaller near interfaces for preciously capturing the temperature and velocity gradient at the boundaries. Commercial software ICEMCFD® is used for discretizing the computational domain into small control volumes.

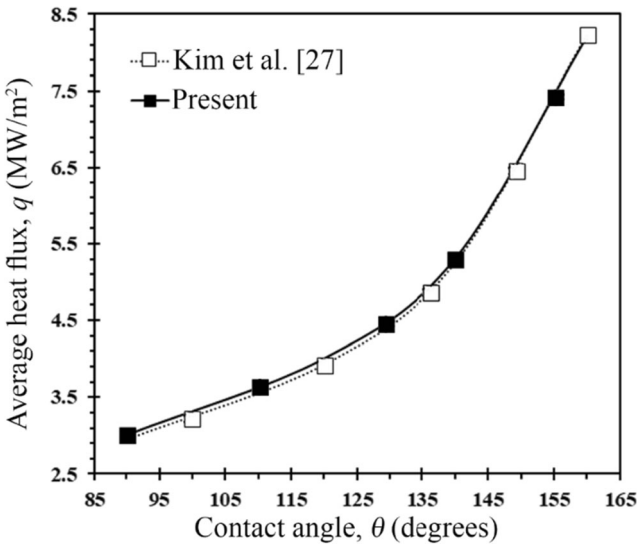

Fig. 4 Average heat flux versus droplet contact angle (θ). Validation carried out for small size droplet (V = 2.5E − 4 nl) considering ΔT = 10 K, T_{sat} = 373 K, δ_c = 0.1 μm, $\hat{\sigma}$ = 0.04 and K_c = 0.2 W/m-K

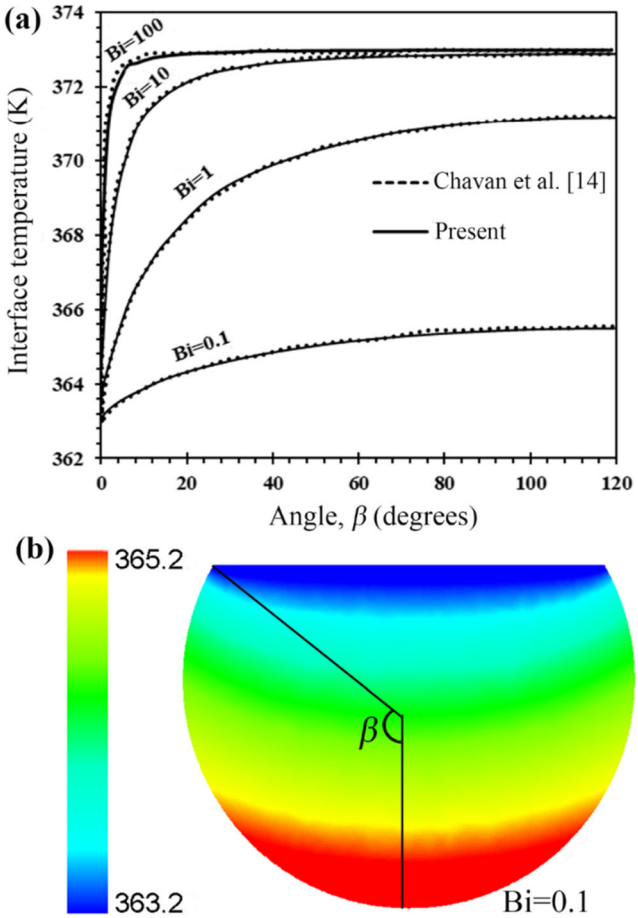

Fig. 5 (**a**) Interface temperature as a function of various interface locations (β) for a droplet in the presence of pure vapor with contact angle (θ) = 120°, $\hat{\sigma}$ = 0.04, T_{sat} = 373 K, ΔT = 10 K and various Biot numbers (0.1 < Bi<100). **b** Temperature contours at the *X*-*Y* plane (Z = 0) of the water droplet shown for Bi = 0.1

The study is performed assuming incompressible fluid of liquid droplet. In addition, the effect of viscous dissipation and leaching of the promoter layer by wall shear stress at the solid-liquid interface is neglected. The governing equation in Cartesian tensor notation are as given in Eqs. (7–9). These equations are solved in Cartesian coordinates using Finite Volume Method (FVM).

$$\frac{\partial u_i}{\partial x_i} = 0 \tag{7}$$

$$\left(\frac{\partial u_i}{\partial t} + \frac{\partial u_j u_i}{\partial x_j}\right) = -\frac{1}{\rho}\frac{\partial p}{\partial x_i} + \frac{\mu}{\rho}\frac{\partial u_i}{\partial x_i^2} + g_i \tag{8}$$

$$\frac{\partial T}{\partial t} + \frac{\partial u_i T}{\partial x_i} = \alpha \frac{\partial^2 T}{\partial x^2} \tag{9}$$

The boundary conditions prescribed at condensing surface and droplet interface are as follows. At the condensing surface, Dirichlet boundary condition and no-slip condition are specified for solving governing equations, i.e. $u = 0$, $v = 0$,

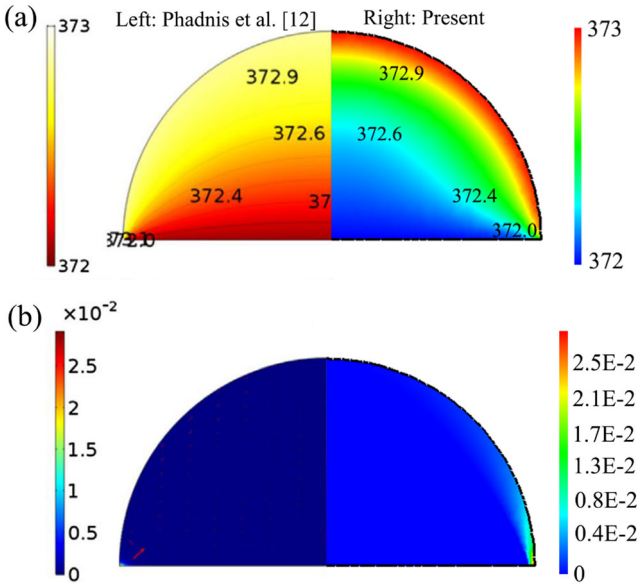

Fig. 6 (**a**) Temperature (K) and (**b**) Marangoni flow velocity (m/s) for Phadnis et al. [12] results (left) and present numerical simulation results (right). The validation study was carried out for a water droplet with Marangoni convection of contact angle (θ) = 90°, r = 1 mm, T_{sat} = 373 K, ΔT = 1 K, $\hat{\sigma}$ = 0.04 and $d\sigma/dT$ = −0.03 mN/m-K

$w = 0$, $T = T_w$ for static droplet. However, $u = U$ is specified for sliding droplet. Here, U is velocity of condensing surface which is equal and opposite to the terminal velocity of sliding droplet [41].

The Marangoni stresses are specified for solving Navier-Stokes equation at the droplet interface. Here, the normal stress is assumed equivalent to vapor pressure however, the shear stresses are estimated using the Eq. (10). The shear stress is zero when Marangoni convection is neglected.

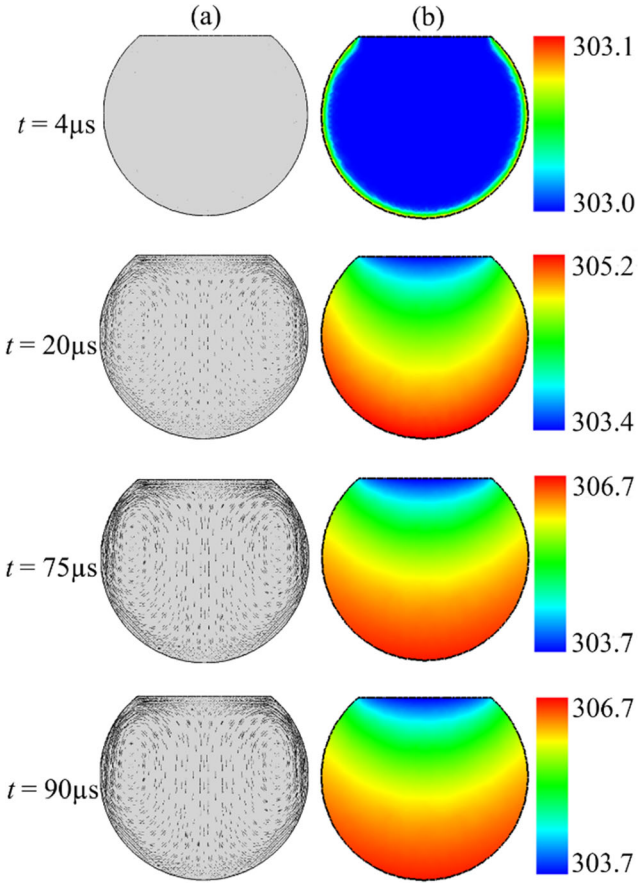

Fig. 8 (**a**) Velocity vector and (**b**) temperature contours on X-Y plane (Z = 0) inside a water droplet (r = 1.77 μm and θ = 140°) with respect to time (t). The numerical simulation preformed considering a droplet in presence of pure vapor with Marangoni convection at T_{sat} = 313 K, $d\sigma/dT$ = −0.13mN/m-K, ΔT = 10 K, $\hat{\sigma}$ = 0.04, δ_w = 0.25 μm, δ_c = 0.1 μm, K_c = 0.2 W/m-K and K_w = 401 W/m-K

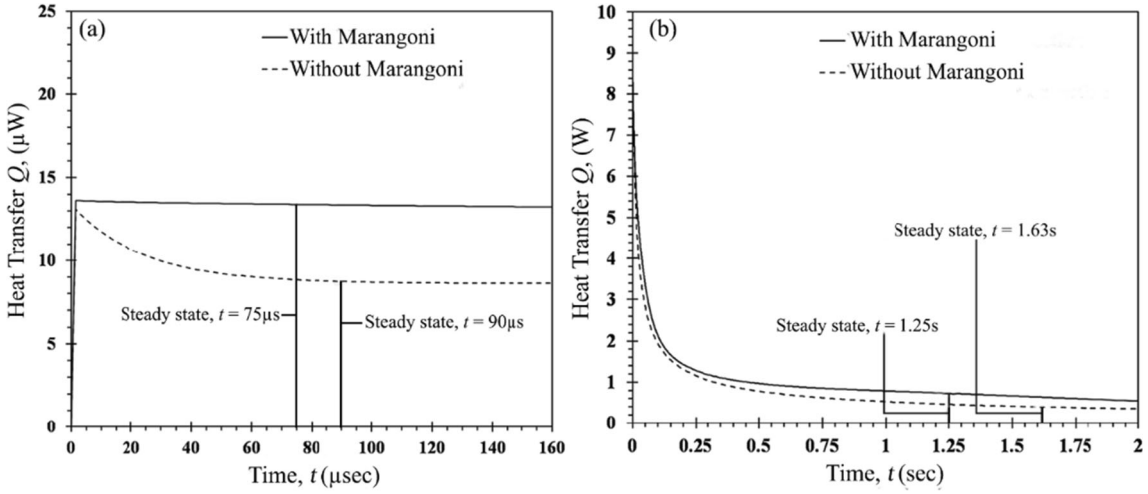

Fig. 7 Heat transfer through water droplet with respect to time (t) for (**a**) small droplet (r = 1.77 μm and V = 2.3E − 04 nl) and (**b**) droplet of maximum possible radius (r = 2.5 mm and V = 630 μl). The numerical simulation was performed with and without Marangoni convection inside the droplet of contact angle (θ) = 140°, T_{sat} = 313 K, ΔT = 10 K, $\hat{\sigma}$ = 0.04, $d\sigma/dT$ = −0.13 mN/m-K, δ_w = 0.25 μm, δ_c = 0.1 μm, K_c = 0.2 W/m-K and K_w = 401 W/m-K

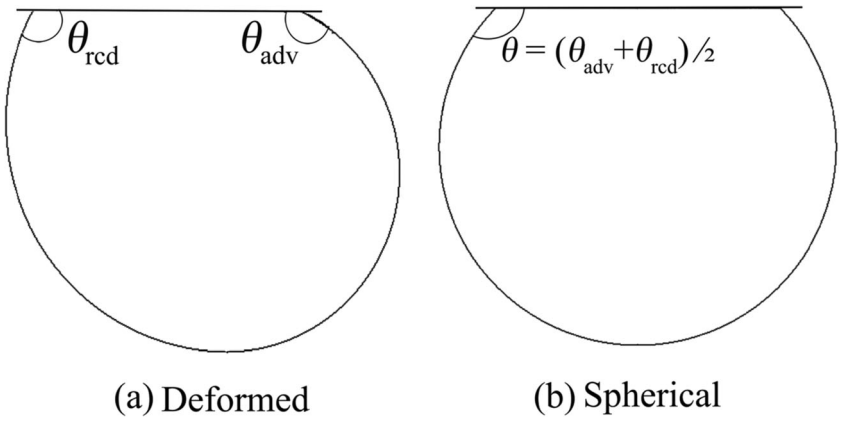

Fig. 9 Schematic diagram of deformed and equivalent spherical cap droplet with equal volume and equal average contact angle

$$\tau_{ji} = \frac{d\sigma_j}{dT}\left(\frac{\partial T}{\partial x_i}\right)_s \tag{10}$$

Here, τ_{ji} is the shear stress (N/m^2), $d\sigma_i/dT$ is the surface tension gradient (N/m-K) and $(\partial T/\partial x_i)_s$ is the temperature gradient at condensing surface (K/m). For solving energy equation at the droplet interface, Robin-Mixed boundary condition is applied, in which constant heat transfer coefficient (h_i) and surrounding vapor temperature is specified. It is assumed that the vapor close to droplet interface i.e. the surrounding vapor is at stagnation state and have temperature equal to capillary temperature (T_{cap}) which is estimated using the capillary resistance of droplet as given in Eq. (11)

$$T_{cap} = T_{sat}\left[1-\frac{2\sigma}{rh_{lv}\rho}\right] \tag{11}$$

The expression for heat transfer coefficient of condensation at droplet interface is estimated as [10].

$$h_i = \left[\frac{2\hat{\sigma}}{2-\hat{\sigma}}\right]\left(\frac{h_{lv}^2\Delta\rho}{T_{sat}}\right)\left(\frac{M}{2\pi\bar{R}T_{sat}}\right)^{1/2}\left[1-\frac{P_v}{\Delta\rho 2h_{lv}}\right] \tag{12}$$

Here, $\hat{\sigma}$ is the condensation coefficient, it is the fraction of striking vapor molecules that will actually condense on the droplet interface, h_{lv} is the latent heat of vaporization (J/kg), $\Delta\rho$ is change in density (kg/m^3), T_{sat} is the saturation temperature of vapor, M is the molecular weight of vapor (kg/mol), $\bar{R}$ is the universal gas constant (J/mol-K) and P_v is the vapor pressure (Pascal) at dew point temperature.

The conjugate heat transfer problem coupled with Navier-stokes equations is solved for three sub-domains using in-house FVM. The details of this solver are reported by the authors elsewhere [13]. Here, validation of the FVM code is discussed against the several experimental and analytical studies. In this solver, the diffusion term is discretized using second-order central difference scheme. However, the convective term is discretized using second-order upwind scheme. Geometry invariant features of the tetrahedral elements are

Table 3 Advancing, receding contact angles of spherical and deformed droplets

S. no.	Volume of droplet (μl)	Contact angle of equivalent spherical cap droplet θ^o	Shape of deformed droplet	
			Advancing contact angle θ_{adv} ^{o}	Receding contact angle θ_{rcd} ^{o}
1	3.59	97	118	75
2		113	142	84
3		134	155	114

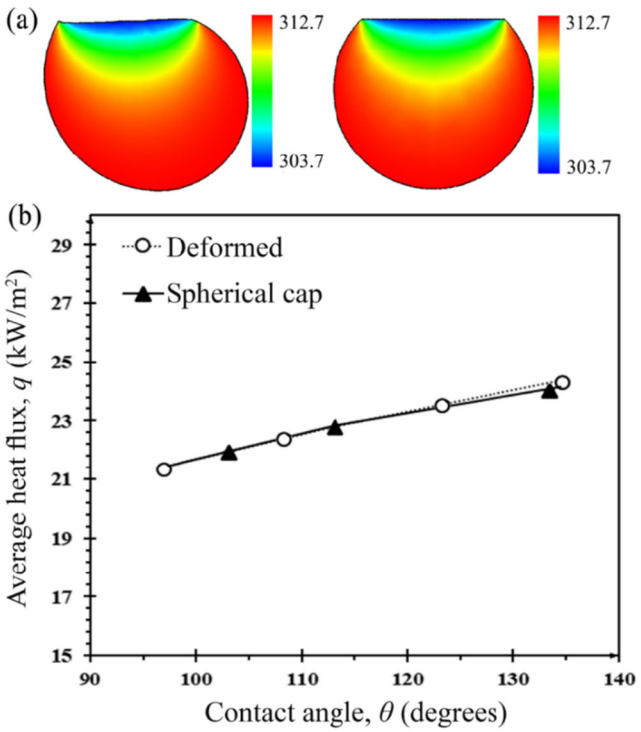

Fig. 10 **a** Temperature contours on X-Y plane ($Z = 0$) of deformed and spherical cap droplet of contact angle (θ) = 134^o. **b** Average heat flux as a function of contact angle for deformed and equivalent spherical cap water droplet; ΔT = 10 K, T_{sat} = 313 K, δ_w = 2 mm, δ_c = 10 μm, $\hat{\sigma}$ = 0.04, V = 3.59 μl, K_c = 0.2 W/m-K and K_w = 401 W/m-K

used so that the calculation of gradients at the cell faces is simplified using nodal quantities of a variable. Nodal quantities, in turn, are calculated as a weighted average of the surrounding cell-centered values. The discretized system of algebraic equation is solved by stabilized bi-conjugate gradient method (biCGStab) with a diagonal precondition. The iterations within the code are executed till an order of convergence = 10^{-07} is achieved for all the computing variables.

The thermo-physical properties of condensing surface and drop promoter layer used in numerical simulation are given in Table 1. However, Table 2 shows the thermo-physical properties of fluids of liquid droplet. This simulation study yields the local wall shear stress and heat flux by knowing the velocity and temperature field of three sub-domains.

3 Results and discussion

Before presenting the outcomes of the present study, grid independent test and validation of the in-house FVM solver are carried out. The simulation is carried out for 2, 4, 5 and 7 lakh tetrahedral elements on static spherical cap shape liquid droplet ($\theta = 140^{o}$, $V = 40$ μl) of Prandtl number 4.32 for examining the optimal grid size. Figure 3 shows the temperature variation at the midline of the liquid water droplet (x-y plane, $z = 0$) with respect to the vertical coordinate for various grid sizes. Numerical simulation is carried out for the droplet with and without Marangoni convection. The results show that a droplet with Marangoni convection, the temperature profile at the midline of the droplet is identical for 5×10^5 and 7×10^5 tetrahedral elements. However, there is no significant effect of consideredgrid size on the temperature profile. Hence, the 5 lakh elements grid is minimum grid size on which solution is independent of grid and this size of grid is chosen in the present study.

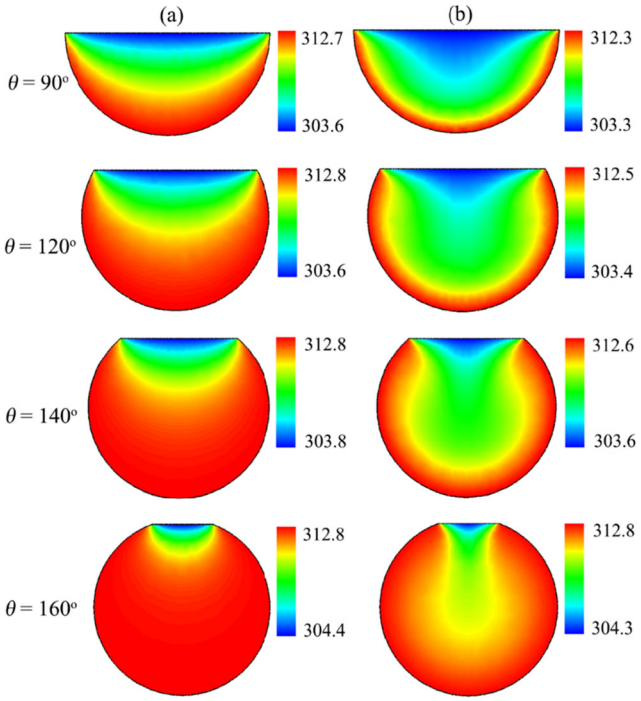

Fig. 12 Temperature contours at X-Y plane ($Z = 0$) inside water droplet at various contact angle; **a** without and **b** with Marangoni convection. The simulation was carried out considering $T_{sat} = 313$ K, $\Delta T = 10$ K, $V = 40$ μl, $\delta_w = 2$ mm, $\delta_c = 10$ μm, $K_c = 0.2$ W/m-K, $K_w = 401$ W/m-K, $d\sigma/dT = -0.13$mN/m-K and $\hat{\sigma} = 0.04$

For validating the FVM-CFD solver, simulations of heat transfer through a droplet have been carried out for conditions reported in the literature [12, 14, 27]. The results obtained from the present study are compared against Kim et al. [27], Chavan et al. [14] and Phadnis et al. [12] data, as shown in Figs. 4, 5, and 6. Figure 4 shows the present simulation data are in good agreement with the results obtained from the analytical model of Kim et al.

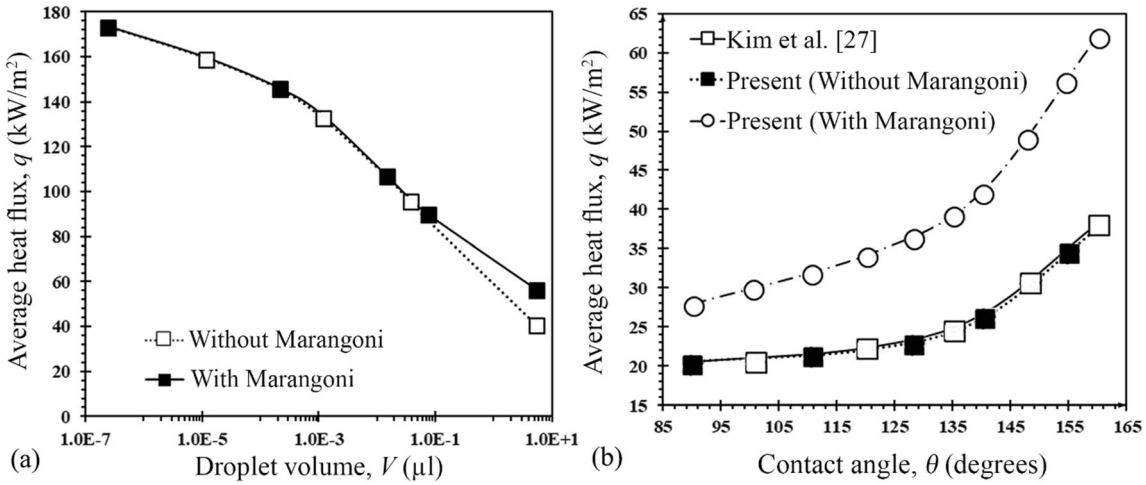

Fig. 11 (**a**) Average heat flux versus droplet volume for droplet with contact angle $\theta = 140^{o}$ and (**b**) effect of Marangoni convection on heat transfer through a droplet. Considering a water droplet with and without Marangoni convection. The study was carried out at operating condition $T_{sat} = 313$ K, $\Delta T = 10$ K, $V = 40$ μl, $\delta_w = 2$ mm, $\delta_c = 10$ μm, $K_c = 0.2$ W/m-K, $K_w = 401$ W/m-K, $\hat{\sigma} = 0.04$ and $d\sigma/dT = -0.13$mN/m-K

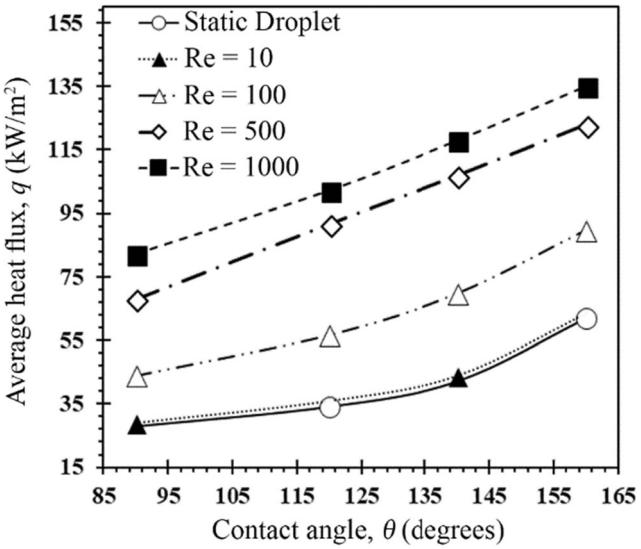

Fig. 13 Variation of average heat flux with respect to droplet contact angle for static and sliding droplet at various Reynolds number. The heat transfer through a sliding water droplet ($V = 40$ μl), estimated for operating conditions $T_{sat} = 313$ K, $\Delta T = 10$ K, $\delta_c = 10$ μm, $\delta_w = 2$ mm, $K_c = 0.2$ W/m-K, $K_w = 401$ W/m-K, $\hat{\sigma} = 0.04$ and $d\sigma/dT = -0.13$mN/m-K

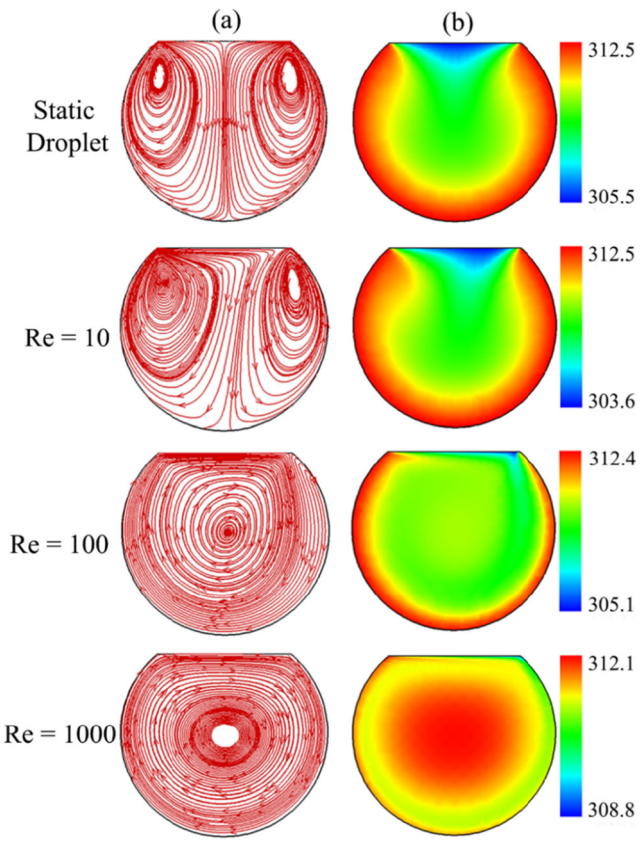

Fig. 14 (**a**) Fluid flow pattern and (**b**) temperature contours at *X-Y* plane ($Z = 0$) inside a water droplet ($V = 40$ μl, $\theta = 140^o$) for static and sliding droplet at various values of Reynolds number. Numerical simulation was performed at $T_{sat} = 313$ K, $\Delta T = 10$ K, $\delta_c = 10$ μm, $\delta_w = 2$ mm, $K_c = 0.2$ W/m-K, $K_w = 401$ W/m-K, $\hat{\sigma} = 0.04$ and $d\sigma/dT = -0.13$mN/m-K

[27]. Figure 5 shows good agreement between the present simulation and Chavan et al. [14] results. Figure 5b shows the temperature profile over the *x-y* plane ($z = 0$) of a water droplet with a contact angle of 120°. This data shows that the maximum temperature is at the apex of the droplet. However, the minimum temperature is at the solid-liquid interface of the droplet which is in accordance with the literature [14]. Further, the Marangoni convection formulation is validated against the numerical study of Phadnis et al. [12]. Figure 6 shows the temperature and Marangoni flow velocity of Phadnis et al. [12] compared with the present numerical simulation. Validation results show good agreement between the present simulation and Phanis et al. [12].

Post-validation, fluid flow and heat transfer simulations for single droplet in static and sliding state are carried out to investigate the effect of various parameters on the heat flux and wall shear stress. The parameters under consideration in this study are time scale to achieve steady state heat transfer, droplet deformation, droplet volume ($V = 2.2\text{E}-07$ μl to 629 μl), thermo-physical properties of liquid droplet (Pr = 0.006 to 189), contact angle ($\theta = 90^o$ to 160^o), interfacial heat transfer coefficient, degree of sub-cooling, thickness and thermal conductivities of the drop promoter layer and condensing surface.

The simulation is carried out to know time-scale to achieve steady state heat transfer for range of drop volume from drop nucleation (2.3 E-04 nl) to droplet slide-off/fall-off (630 μl). Figures 7 and 8 shows time-scale to achieve steady state when heat is transferred through the liquid droplet of various sizes, with and without Marangoni convection. Figure 7a shows the variation of heat transfer rate with respect to the time (*t*) for small droplet ($r = 1.77$ μm). However, Fig. 7b shows the variation of heat transfer rate for maximum possible droplet radius ($r = 2.5$ mm) on/underneath the condensing surface. Results show that small droplet reaches steady state in 75 μs whereas, large droplet reaches steady state in time close to 1 s. Hence, considering the steady state heat transfer through the droplet on convectional time scale is appropriate and drop achieve steady state faster when there is Marangoni convection. Figure 8 (a-b) shows the variation of velocity vectors and temperature contours on *X-Y* plane ($Z = 0$) from initial time step ($t = 0$) to the time it reaches steady state for 1.77 μm droplet with Marangoni. It also shows that there is no qualitative change in velocity vector and temperature contour after 75 μs.

In general, the droplet deforms on or underneath an inclined surface due to imbalance in the forces, i.e. when the gravity force overcomes surface tension at the liquid-vapor interface to achieve the necessary static balance. To investigate the effect of drop deformation with respect to its equivalent spherical cap drop on heat transfer rate, the simulation is carried out for a static deformed droplet and its equivalent spherical cap droplet. Figure 9a and b shows the schematic diagram of deformed droplet and equivalent spherical cap

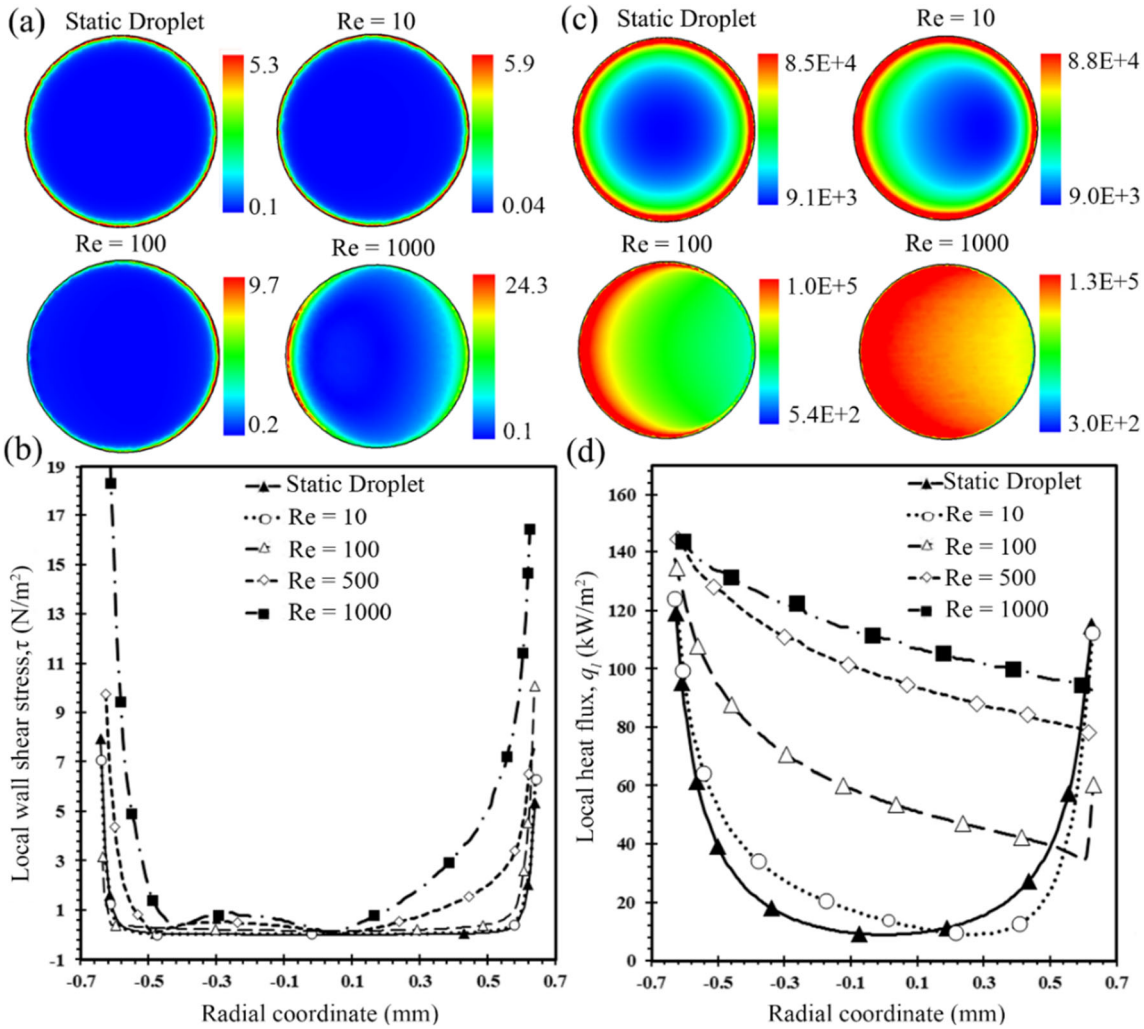

Fig. 15 (**a**–**b**) Local wall shear stress and **c**–**d** local heat flux distribution at X-Z ($Y = 0$) plane, parallel to the condensing surface of static and sliding droplet with contact angle $\theta = 140^{o}$ at various Reynolds number. Numerical simulation was carried out considering $T_{sat} = 313$ K, $\Delta T = 10$ K, $\delta_c = 10$ μm, $\delta_w = 2$ mm, $K_c = 0.2$ W/m-K, $K_w = 401$ W/m-K, $\hat{\sigma} = 0.04$ and $d\sigma/dT = -0.13$mN/m-K

droplet respectively. The equivalent spherical cap droplet has volume equal to deformed droplet and contact angle equal to average of advancing and receding angles of deformed droplet. The shape and size of deformed droplet and its equivalent spherical cap droplet considered in this study are showed in Table 3. Figure 10a shows that the temperature contours on X-Y plane of deformed and equivalent spherical cap droplet are identical. Figure 10b shows the variation of average heat flux for various shapes of deformed and its equivalent spherical cap droplet. This shows that the average heat flux is equal for a deformed droplet and equivalent spherical cap droplet however, it varies for various contact angle of droplet. Therefore, considering the spherical cap shape of droplet in place of deform drop on inclined surface is appropriate in the modelling of heat transfer through the droplet in dropwise condensation.

The average heat flux versus droplet volume (V) and the average heat flux versus droplet contact angle (θ) are plotted to investigate the significance of Marangoni convection, as shown in Fig. 11. Figure 11a shows the variation of average heat flux with respect the droplet volume (V). Results show that the heat flux increases as the droplet volume decreases. However, the effect of Marangoni convection dominant for droplet volume (V) ≥ 0.034 μl (Ma ≥ 2204). Figure 11b shows that the average heat flux for a 40 μl droplet with Marangoni convection is approximately twice as compared to droplet of same volume without Marangoni convection. This plot also shows the comparison of Kim et al. [27] with present simulation data, without Marangoni convection. The constriction resistance (R_{const}) was neglected by Kim et al. [27]. However, present simulation is performed considering all the thermal resistances. Generally, the heat transfer through liquid droplet decreases as the constriction resistance is taken into consideration. However, there is no significant difference between Kim et al. [27] and results of present simulation without Marangoni. Hence, this study also concludes that the effect of constriction

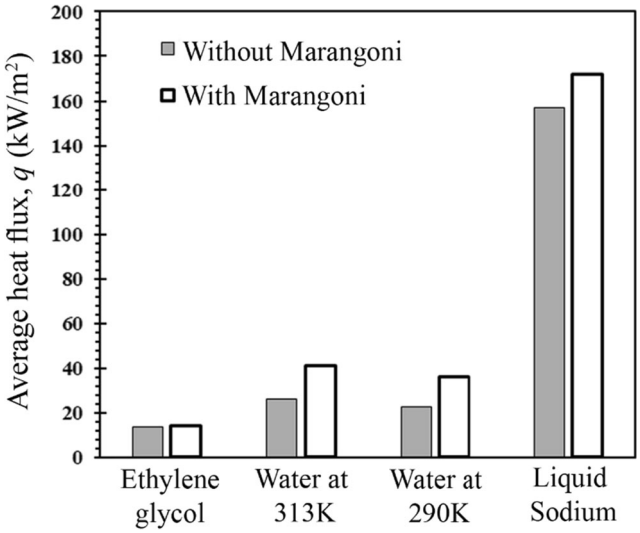

Fig. 16 Average heat flux for droplet of various Prandtl number fluids ($V = 40$ µl), with and without Marangoni convection. The numerical simulation was carried out considering droplet with contact angle $\theta = 140^{o}$, $\Delta T = 10$ K, $\delta_c = 10$ µm, $\delta_w = 2$ mm, $K_c = 0.2$ W/m-K, $K_w = 401$ W/m-K and $\hat{\sigma} = 0.04$

resistance is negligible during heat transfer from water droplet to the copper condensing surface of thickness ≤ 2 mm.

Figure 12a–b shows the temperature contours with and without Marangoni convection on X-Y plane ($Z = 0$) for various shapes of 40 µl droplet. The droplet with Marangoni of various shapes has uniform temperature distribution which leads to the formation of a recirculating flow inside the droplet, due to this reason the temperature gradient at interface is more with Marangoni as compared to droplet without Marangoni and this leads to enhance heat transfer rate through liquid droplet with Marangoni convection as shown in Fig. 11b.

Figures 13, 14, and 15 show the comparison of convection (sliding spherical cap droplet) and Marangoni convection (static spherical cap droplet) on the heat flux and wall shear stress for a liquid droplet (Pr = 4.32). The sliding droplet is considered at various Reynold number (Re) = 10, 100, 500 and 1000. However, the volume of sliding and static droplet is assumed equal in the simulation.

Figure 13 shows variation of average heat flux for a static and a sliding droplet at various contact angles of droplet. Figure 14 shows the fluid flow pattern and temperature contours at X-Y plane ($Z = 0$) of the static and sliding liquid droplet. The pattern of streamlines in droplet that is otherwise stationary is different when compared to the streamline patterns in a sliding droplet when Re ≥10. Increasing Reynolds number is indicative of increasing inertia, a source of nonlinearity that breaks symmetry in velocity and temperature distribution. In addition, drop shapes change with drop volume as well as the angle of inclination, yielding distinct levels of asymmetry. In real terms, the main-flow velocity within the drop tends to zero as one approach the condensing surface. However, in this work the frame of reference is fixed to the liquid droplet and the condensing surface moves relative to it at constant speed. Reynolds number for given liquid droplet depends on the velocity of the condensing surface. Inertia, buoyancy and surface tension gradient forces are responsible for asymmetric circulation of the liquid inside the droplet. For a static drop (Re = 0), inertia force is zero. Therefore, temperature distribution is symmetric with respect to the drop height. However, surface tension gradient force and inertia force act simultaneously in a sliding droplet. Hence, the flow is not

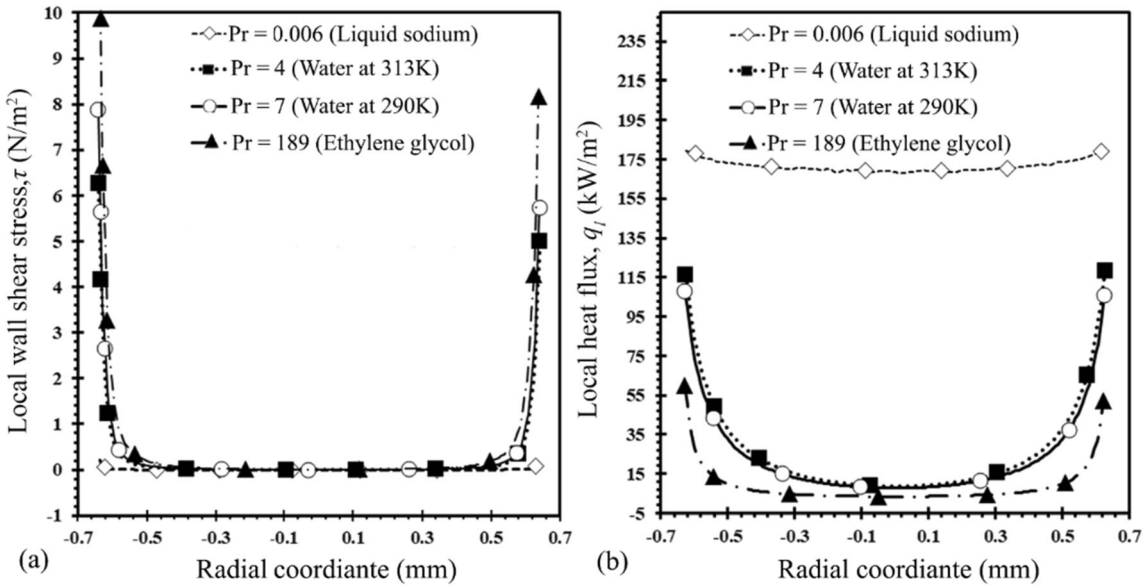

Fig. 17 (**a**) Local wall shear stress and (**b**) local heat flux distribution on the condensing substrate of droplet with contact angle $\theta = 140^{o}$ for fluids of various Prandtl numbers (Pr = 0.006, 4, 7 and 189). Numerical simulation was carried out considering $T_{sat} = 313$ K, $\Delta T = 10$ K, $V = 40$ µl, $\delta_w = 2$ mm, $\delta_c = 10$ µm, $K_c = 0.2$ W/m-K, $K_w = 401$ W/m-K and $\hat{\sigma} = 0.04$

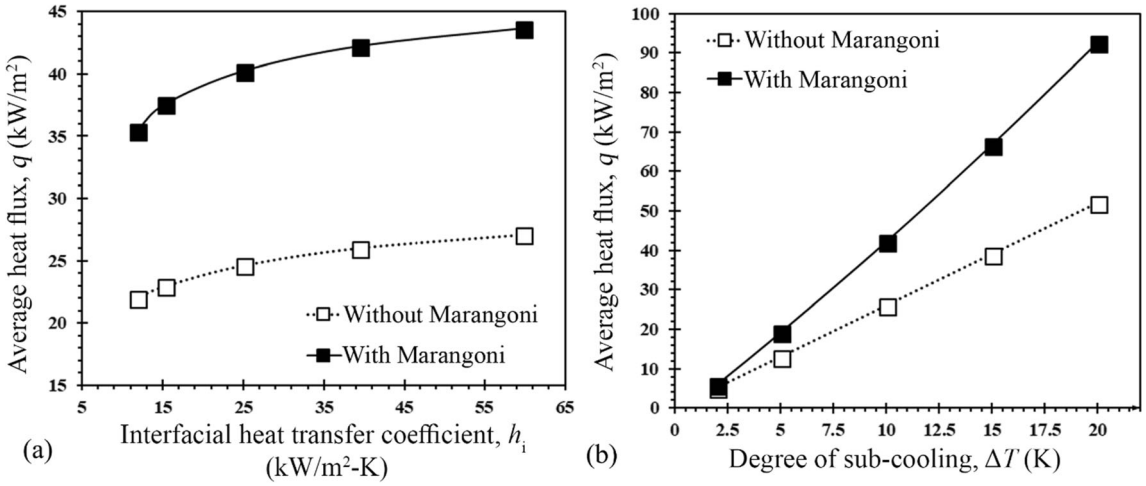

Fig. 18 Variation of average heat flux with respect to (**a**) interfacial heat transfer coefficient at $\Delta T = 10$ K and (**b**) degree of sub-cooling at $\delta_w = 2$ mm, $\delta_c = 10$ μm, $\theta = 140^o$, $V = 40$ μl, $d\sigma/dT = -0.13$mN/m-K and $\hat{\sigma} = 0.04$

symmetric with respect to the vertical coordinate. As Re increases, the centroid of flow circulation shifts towards the wall and flow becomes increasingly unsymmetric due to unequal advancing and receding angles.

Figure 15 a and c shows the contours for local wall shear stress and local heat flux on the *X*-*Z* plane ($Y = 0$). However, Fig. 15b and d shows the variation of local wall shear stress and local heat flux along the base diameter of the droplet (radial coordinate). Local wall shear stress and local heat flux are minimum at the central region of foot-print of solid-liquid interface. However, their maximum value is at three-phase contact line. It is observed that the maximum value of local heat flux and local wall shear stress shift towards left periphery of the solid-liquid interface when droplet slide-off.

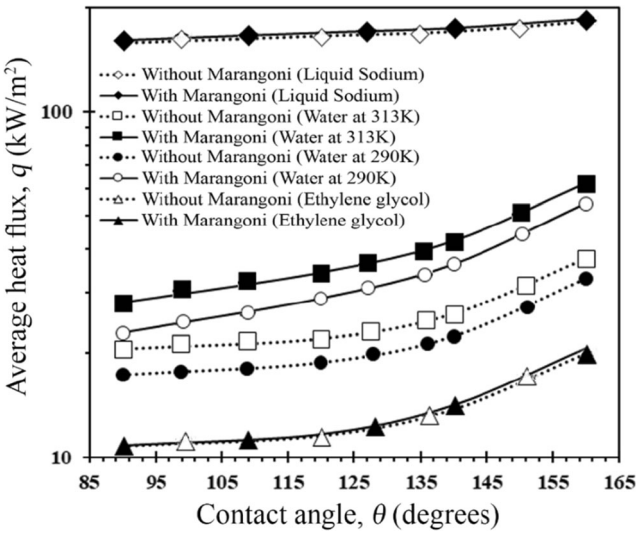

Fig. 19 Average heat flux versus contact angle of a droplet of various fluids with and without Marangoni convection, considering $\Delta T = 10$ K, $V = 40$ μl, $\delta_w = 2$ mm, $\delta_c = 10$ μm, $\hat{\sigma} = 0.04$, $T_{sat} = 313$ K, $K_c = 0.2$ W/m-K and $K_w = 401$ W/m-K

Figure 15b and d also show that these transport coefficients increase with increasing Reynolds number.

Figure 16 compares the average heat flux with Marangoni (white bar) and without Marangoni (gray bar) for liquid droplets with varying thermo-physical properties. These liquids are sodium (Pr = 0.006), water (Pr = 4.32 and 7) and ethylene glycol (Pr = 189). Graph shows that there is negligible effect of Marangoni in heat transfer through ethylene glycol droplet. However, the water droplet (Pr = 4.32) has maximum effect of Marangoni convection. Liquid sodium droplet has high heat transfer rate as compared to other liquids droplet. Therefore, it can be concluded that the average heat flux increases as the Prandtl number of fluid decreases.

Figure 17a-b shows the local wall shear stress and local heat flux variation along the droplet base diameter of 40 μl droplet for various fluids of liquid droplet. The local heat flux decreases however, the local wall shear stress increases with increasing Prandtl number of liquid droplet.

Figure 18a-b shows effect of interfacial heat transfer coefficient and degree of sub-cooling on average heat flux. The average heat flux gradually increases with increase in interfacial heat transfer coefficient due to very small reduction in the interfacial resistance. However, the average heat flux increases linearly with increasing degree of sub-cooling. The slop of average heat flux with respect to degree of sub-cooling is more for droplet with Marangoni convection.

The effect of contact angle, condensing surface and promoter layer thickness and conductivities on the heat transfer through a static droplet, for various fluids of liquid droplet is shown in Figures 19, 20, and 21. Figure 19 shows the variation of average heat flux with respect to contact angle for a droplet. Results show that average heat flux is a strong function of contact angle and it increases as contact angle increases. Hence, super-hydrophobic surfaces are preferred for enhancing the average heat flux in dropwise condensation.

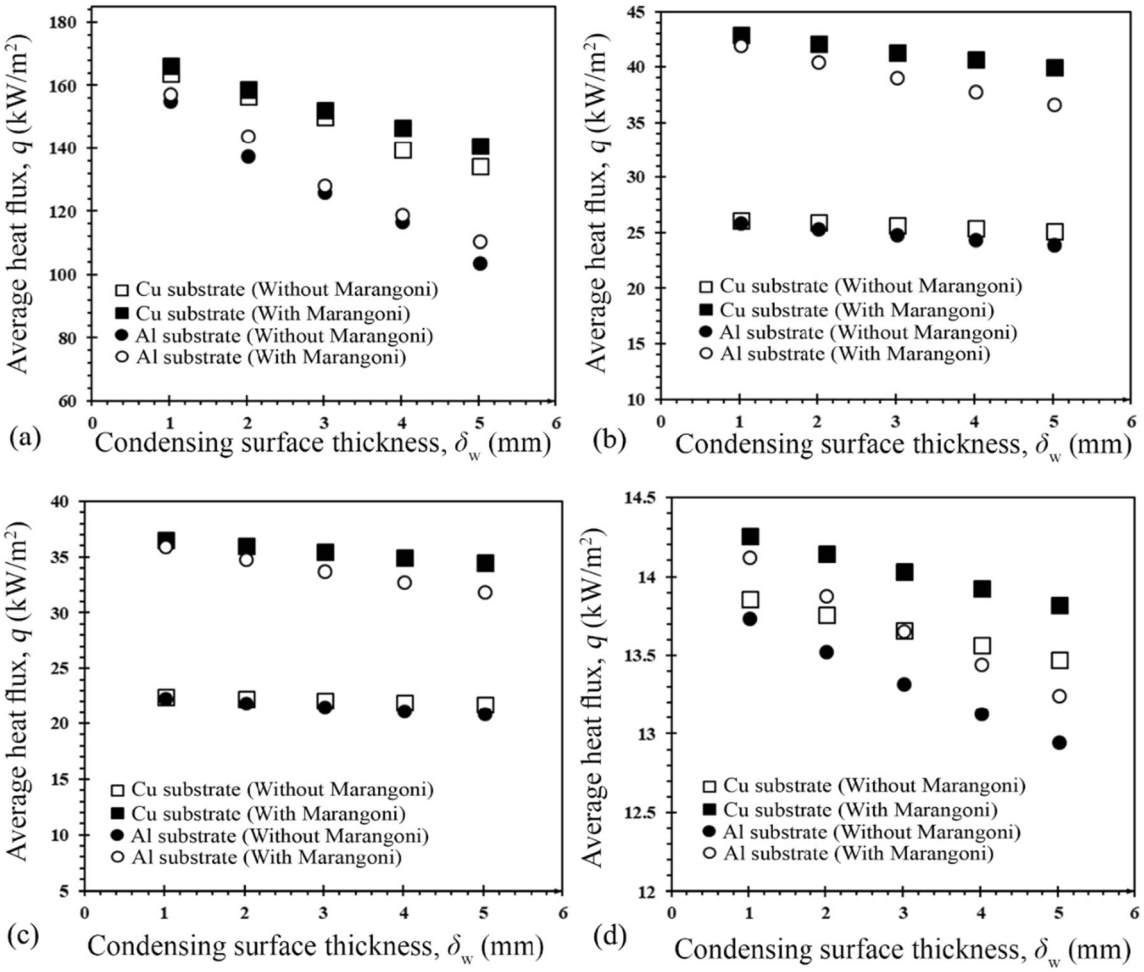

Fig. 20 Average heat flux with respect to condensing surface thickness for copper and aluminum surfaces for droplet of various fluid; **a** liquid sodium (Pr = 0.006), **b** water at 313 K (Pr = 4), **c** water at 290 K (Pr = 7) and **d** ethylene glycol (Pr = 189). Numerical simulation was carried out considering $\Delta T = 10$ K, $\delta_c = 10$ μm, $\theta = 140^o$, $V = 40$ μl and $\hat{\sigma} = 0.04$

The effect of thermal conductivities and thickness of condensing surface on the average heat flux is shown in Fig. 20a-d. In this study, the condensing surfaces are of Copper (401 W/m-K) and Aluminum (180 W/m-K) with a thickness ranging from 1 to 5 mm. The results show that average heat flux increases as the thermal conductivity of the condensing

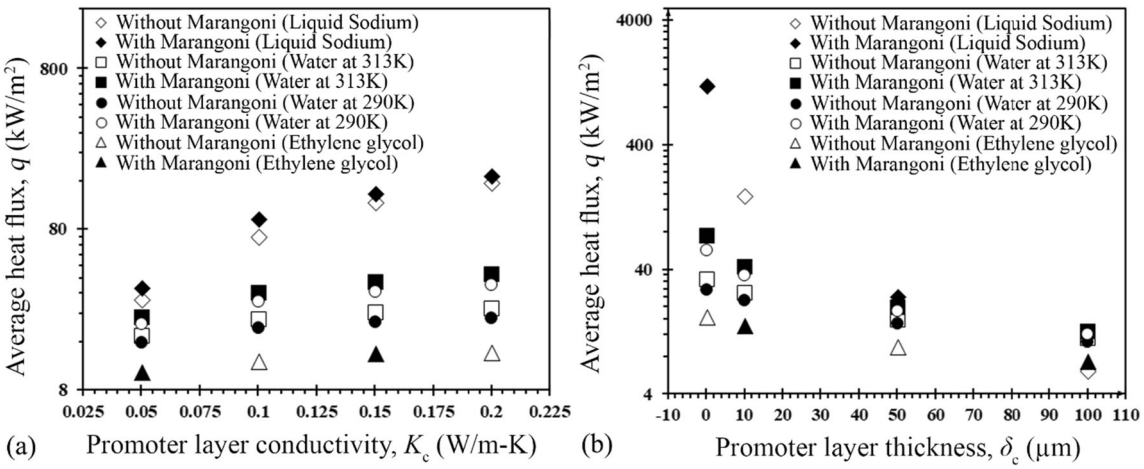

Fig. 21 Variation of average heat flux for $\Delta T = 10$ K, $T_{sat} = 313$ K, $\delta_w = 2$ mm, $\theta = 140^o$, $V = 40$ μl and $\hat{\sigma} = 0.04$. **a** Effect of thermal conductivity of promoter layer at $\delta_c = 10$ μm and **b** effect of promoter layer thickness

surface increases. However, it decreases as thickness of the condensing surfaces increases. The average heat flux decreases at faster rate for liquid sodium and ethylene glycol droplet as compared water droplet.

Figure 21a-b shows effect of thermal conductivity and thickness of drop promoter layer on average heat flux. Results show that average heat flux decreases as the thickness of promoter layer increases. However, average heat flux increases as the thermal conductivity of promoter layer increases.

Finally, present simulation study shows that contact angle, droplet volume, degree of sub-cooling, interfacial heat transfer coefficient, drop instability, Marangoni convection, thermophysical properties of liquid droplet, thickness and thermal conductivities of drop promoter layer and condensing surface plays a crucial role in heat transfer through the droplet interface to condensing surface in dropwise condensation.

4 Summary and conclusions

A numerical simulation of heat transfer through a liquid droplet, considering all the thermal resistances has been reported. The resistances considered were interfacial, capillary, conduction, Marangoni, convection, drop promoter layer and constriction resistances. In this study, the coupled 3-D Navier-Stokes and energy equations were solved for three-subdomain simultaneously using in-house FVM solver. The results obtained from the in-house CFD solver were validated against data available in the literature which were found in good agreement. Post-validation, a parametric study was performed to investigate the heat flux and wall shear stress during heat transfer through a droplet of various Prandtl number fluid. Following conclusions have been drawn from the study.

- The heat transfer through droplet to the condensing surface achieves steady state in microsecond time scale. Therefore, assuming steady state at conventional time scale is appropriate.
- The heat flux of deformed and equivalent spherical cap droplet is equal. Therefore, assuming spherical cap droplet despite deform droplet is appropriate.
- The sliding droplet study concludes that the heat transfer through a sliding droplet is majorly dominated by convection mode of heat transfer.
- Marangoni convection significantly enhances the heat transfer through droplet when $Ma \geq 2204$.
- The constriction resistance can be neglected for copper condensing surface of thickness ≤ 2 mm.
- A superhydrophobic metallic surface is an appropriate substrate for enhancing the heat transfer rate through a liquid droplet.
- The average heat flux increases as the liquid droplet condenses on thin and highly conductive drop promoter layer and condensing surface in presence of vapor with high values of saturation temperature and degree of sub-cooling
- The heat flux increases with increasing Reynolds number of sliding droplet and decreasing Prandtl number of static liquid droplet.

Acknowledgments The authors acknowledge the financial support from Science and Engineering Research Board (SERB), Department of Science and Technology (DST), Govt. of India (Project No. ECR/2016/000020).

Compliance with ethical standards

Conflict of interest The authors declare that they have no conflict of interest.

Publisher's Note Springer Nature remains neutral with regard to jurisdictional claims in published maps and institutional affiliations.

References

1. Bhardwaj R, Ten Kortenaar MV, Mudde RF (2013) Influence of condensation surface on solar distillation. Desalination 326:37–45
2. Liu L, Jacobi AM (2006) The effects of hydrophilicity on water drainage and condensate retention on air-conditioning evaporators. Presented at the International Refrigeration and Air Conditioning Conference
3. Khawaji AD, Kutubkhanah IK, Wie JM (2008) Advances in seawater desalination technologies. Desalination 221:47–69
4. Al-Khayat O, Hong JK, Beck DM, Minett AI, Neto C (2017) Patterned polymer coatings increase the efficiency of dew harvesting. ACS Appl Mater Interfaces 9:13676–13684
5. Schmidt VE, Schurig W, Sellschopp W (1930) Versuche uber die Kondensation von Wasserdampf in Film- und Tropfenform. Forsch Ingenieurwes 1:53–63
6. Le Fevre EJ, Rose JW (1965) An experimental study of heat transfer by dropwise condensation. Int J Heat Mass Transf 8:1117–1133
7. Graham C, Griffth P (1973) Drop size distribution and heat transfer in dropwise condensation. Int J Heat Mass Transf 16:337–346
8. Leipertz A., Koch G (1998) Dropwise condensation of steam on hard coated surfaces. In: XIth Int. Heat Transfer Conf, p 379–384
9. Eucken A (1937) Energie und stoffaustausch an grenzflächen", Energy and mass transfer at interfaces, 25:209–219
10. Carey VP (2008) Liquid-vapor phase-change phenomena", second edition Taylor and Francis Group, LLC, New York:45–472
11. Tanasawa I (1991) Advance in condensation heat transfer, Advances in Heat Transfer (ed.: Hartnett JP, Irvine TF, and Cho IY), 21:56–136.
12. Phadnis A, Rykaczewski K (2017) The effect of Marangoni convection on heat transfer during dropwise condensation on hydrophobic and omniphobic surfaces. Int J Heat Mass Transf 115:148–158
13. Sikarwar BS, Khandekar S, Muralidhar K (2013) Simulation of flow and heat transfer in a liquid drop sliding underneath a hydrophobic surface. Int J Heat Mass Transf 57:786–811
14. Chavan S, Cha H, Orejon D, Nawaz K, Singla N, Yeung YF, Park D, Kang DH, Chang Y, Takata Y, Miljkovic N (2016) Heat transfer

through a condensate droplet on hydrophobic and nanostructured superhydrophobic surfaces. Langmuir 32:7774–7787
15. Thickett SC, Neto C, Harris AT (2011) Biomimetic surface coatings for atmospheric water capture prepared by Dewetting of polymer films. Adv Mater 23:3718–3722
16. Varshney P, Mohapatra S, Kumar A (2017) Fabrication of mechanically stable superhydrophobic aluminium surface with excellent self-cleaning and anti-fogging properties. Biomimetics 2:2
17. Huang Y, Sarkar DK, Grant CX (2010) A one-step process to engineer superhydrophobic copper surfaces. Mater Lett 64:2722–2724
18. Miljkovic N, Wang EN (2013) Condensation heat transfer on superhydrophobic surfaces. MRS Bull 38:397–406
19. Enright R, Miljkovic N, Dou N, Nam Y, Wang EN (2013) Condensation on superhydrophobic copper oxide nanostructures. J Heat Transf 135:091304
20. Chen X, Weibel JA, Garimella SV (2015) Exploiting microscale roughness on hierarchical superhydrophobic copper surfaces for enhanced dropwise condensation. Adv Mater Interfaces 2:1–6
21. Bansal GD, Khandekar S, Muralidhar K (2009) Measurement of heat transfer during drop-wise condensation of water on polyethylene. Nanosc Microsc Therm Eng 13:184–201
22. Glicksman LR, Hunt AW (1972) Numeical simulation of dropwise condensation. Int J Heat Mass Transf 15:2251–2269
23. Abu-Orabi M (1998) Modelling of heat transfer in dropwise condensation. Int J Heat Mass Transf 41:81–87
24. Fatica N, Katz DL (1949) Dropwise condensation. Chem Eng Prog 45:661–674
25. Le Fevre EJ, Rose JW (1966) A theory of heat transfer by dropwise condensation. Presented at the Third International Heat Transfer Conference, Chicago
26. Sikarwar BS, Khandekar S, Muralidhar K (2013) Mathematical modelling of dropwise condensation on textures surfaces. Sadhana 36:1135–1171
27. Kim S, Kim KJ (2011) Dropwise condensation modeling suitable for superhydrophobic surfaces. J Heat Transf 133:081502
28. Rykaczewski K (2012) Microdrolet growth mechanism during water condensation on superhydrophobic surfaces. Langmuir 28:7720–7729
29. Miljkovic N, Enright R, Wang EN (2013) Modeling and optimization of superhydrophobic condensation. J Heat Transf 135:111004
30. Kim H, Nam Y (2016) Condensation behaviors and resulting heat transfer performance of nano-engineered copper surfaces. Int J Heat Mass Transf 93:286–292
31. Liu X, Cheng P (2015) Dropwise condensation theory revisited: part I. droplet nucleation radius. Int J Heat Mass Transf 83:833–841
32. Talesh B, Hamid R, Saffari H (2017) Mathematical modeling and numerical simulation of dropwise condensation on an inclined circular tube. J Aerosp Technol Manag 9:476–488
33. Rose JW (1981) Dropwise condensation theory. Int J Heat Mass Transf 24:191–194
34. Guadarrama-Cetina J, Narhe RD, Beysens DA, Gonzalez-Vinas W (2014) Droplet pattern and condensation gradient around a humidity sink. Phys Rev E Stat Nonlinear Soft Matter Phys 89:012402
35. Vemuri S, Kim KJ (2006) An experimental and theoretical study on the concept of dropwise condensation. Int J Heat Mass Transf 49:649–657
36. Hu HW, Tang GH, Niu D (2015) Experimental investigation of condensation heat transfer on hybrid wettability finned tube with large amount of non-condensable gas. Int J Heat Mass Transf 85:513–523
37. Adhikari S, Nabil M, Rattner AS (2017) Condensation heat transfer in a sessile droplet at varying biot number and contact angle. Int J Heat Mass Transf 115:926–931
38. Sikarwar BS (2012) Modeling dropwise condesation underneath inclined textured surfaces. Doctor of Philosophy, Department of Mechanical Engineering, Indian Institute of Technology Kanpur, Kanpur, India
39. Elsherbini AI, Jacobi AM (2004) Liquid drops on vertical and inclined surface II: an experimental study of drop geomerty. J Colloid Interface Sci 273:566–575
40. Elsherbini AI, Jacobi AM (2004) Liquid drops on vertical and inclined surface I: an experimental study of drop geomerty. J Colloid Interface Sci 273:556–565
41. Kim HY, Lee H, Kang BH (2002) Sliding of drops down an inclined solid surface. J Colloid Sci 247:372–382
42. Valencia JJ, Peter N (2008) ASM handbook, ASM International, Casting, 15:468–481
43. Incropera PF, Dexitt PD (2007) Fundamentals of heat and mass transfer, Fourth ed. John Wiley and Sons Inc., New York, 1996
44. Tsuruta T, Kato Y (1994) Estimation of condensation coefficient by dropwise condensation method (condensation coefficients of ethylene glycol and water), The Japan Society of Mechanical Engineers, 60(570):158–164